Available online at www.sciencedirect.com
SCIENCE DIRECT
Catalysis Today 112 (2006) 117–120
CATALYSIS TODAY
www.elsevier.com/locate/cattod

Effect of the nature and structure of pillared clays in the catalytic behaviour of supported manganese oxide

A. Gil [a,*], M.A. Vicente [b], S.A. Korili [a]

[a] *Departamento de Química Aplicada, Edificio Los Acebos, Universidad Pública de Navarra, Campus de Arrosadía, s/n, E-31006 Pamplona, Spain*
[b] *Departamento de Química Inorgánica, Facultad de Ciencias Químicas, Universidad de Salamanca, Plaza de la Merced, s/n, E-37008 Salamanca, Spain*

Available online 6 January 2006

Abstract

In the present work, the complete oxidation of acetone has been studied over a series of supported manganese oxide catalysts on the unpillared and the Al- and Zr-pillared forms of two natural clays, a montmorillonite and a saponite. A significant influence of the clay supports characteristics on the catalytic performance has been found. The following order of improving catalytic performance is established with respect to the pillars composition: Al-pillared clays < unpillared clays < Zr-pillared clays.

Keywords: Acetone complete oxidation; Alumina-pillared clays; Manganese oxide catalysts; Pillared clays; Zirconia-pillared clays

1. Introduction

The catalytic combustion is an effective technology for controlling volatile organic compounds (VOCs) emissions, which has been successfully used in a variety of industrial applications. In this process, very high destructive efficiencies can be achieved at relatively low operating temperatures resulting in considerable environmental and economic benefits in comparison to the case of the more conventional thermal regenerative oxidation.

In contrast to the case of the high-temperature catalytic combustion for gas turbines, relatively little attention has been paid to the support materials for low-temperature applications [1–3]. In addition to the effects related to the dispersion of the active phase, the support can play a role in other important factors conditioning the performance in catalytic combustion. Particularly, remarkable effects have been attributed to the acid sites of the support because of their participation in complementary bifunctional steps involved in the process, in the transformation of VOCs towards reactive organic intermediates and preventing the oxidation of supported noble metals [4–8].

In the present work, the effect of the nature and structure of several alumina- and zirconia-pillared clays as supports of manganese oxide catalysts for the complete oxidation of acetone is studied.

2. Experimental

Two natural clay minerals were used as raw materials, a saponite from Ballarat (California, USA) and a montmorillonite from Gador (Almería, Spain). The clays have been intercalated with Al and Zr hydroxy-polycations using a conventional intercalating procedure [9]. The pillared clays, after calcination at 500 °C, were used as supports. The supported manganese oxide catalysts were prepared by incipient wetness impregnation of the supports with the required volume of an aqueous solution of $Mn(NO_3)_2{\cdot}4H_2O$ (Merck, p.a.) in order to obtain catalysts with a final MnO_2 content of about 10 wt.%. The impregnated solids were subsequently dried at 120 °C for 16 h and calcined at 500 °C for 4 h. The original clays, also calcined at 500 °C, were tested as supports as well. The catalysts are referred in Mn/clay support notation (e.g., Mn/BAsap, Mn/GAmont-Al, Mn/BAsap-Zr, etc.). GAmont and BAsap with reference to the

* Corresponding author. Tel.: +34 948 169602; fax: +34 948 169602.
E-mail address: andoni@unavarra.es (A. Gil).

0920-5861/$ – see front matter © 2005 Elsevier B.V. All rights reserved.
doi:10.1016/j.cattod.2005.11.046

unpillared clay, clay-Al and clay-Zr with reference to the intercalation solution used.

The solids were characterized by chemical analysis, X-ray diffraction (XRD) analysis, N_2 adsorption at −196 °C, and TPR analysis. The phases present in the synthesised solids were identified by XRD analysis on a Siemens D-500 Powder Diffractometer, using nickel-filtered Cu Kα (λ = 1.5405 Å) radiation. Nitrogen adsorption experiments were performed at −196 °C with use of a static volumetric apparatus (Micromeritics ASAP 2010 Adsorption Analyser). The samples were previously degassed at 200 °C for 24 h. Nitrogen adsorption data were obtained with the use of 0.2 g of sample and successive doses of nitrogen of 4 cm^3/g measured at STP conditions until $p/p^\circ = 0.01$ was reached. Each data of adsorption was equilibrated for at least 2 h in order to characterize correctly the smallest micropores. Subsequently, further nitrogen was added and the volume required to achieve a fixed set of p/p° was measured. Only the nitrogen adsorption data up to a relative pressure of 0.2 were considered in the micropore characterization. Temperature-programmed reduction (TPR) analysis was carried out in a Micromeritics TPR/TPD 2900 instrument, from room temperature to 700 °C, with a heating rate of 10 °C/min, under a total flow of 25 cm^3/min (5% H_2 in Ar, Air Liquide). Amounts of about 30 mg were used in the experiments. Water and other compounds that may be formed during the metal reduction and precursor decomposition were trapped using an isopropanol slurry to avoid interference with the measured signal. Hydrogen consumption was measured by a thermal conductivity detector (TCD) and the calibration of the TCD was performed using Ag_2O as external reference.

The acetone combustion reaction was carried out in a tubular fixed-bed Pyrex glass reactor at atmospheric pressure [4]. The light-off curves for acetone combustion were obtained at a controlled heating rate of 2.5 °C/min and a GHSV of 34,000 h^{-1}, based on the total catalytic bed volume. The runs were performed at a W_{Mn}/F_{in} ratio of 0.40 g_{Mn} min/$mmol_{acetone}$. The feed always consisted of 600 ppm acetone in air and on-line analysis of the product stream was performed on a Hewlett-Packard 6890 gas chromatograph.

3. Results and discussion

The basal spacing of the pillared solids prepared in this work and used as metal supports, varied between 1.83 and 2.05 nm. The data were determined from the (0 0 1) reflection in the powder XRD patterns.

The nitrogen adsorption isotherms of the all pillared materials were of type I in the Brunauer, Deming, Deming and Teller (BDDT) classification [10]. The manganese oxide catalysts supported on Al- and Zr-PILCs exhibited specific total surface areas and total pore volumes between 180 and 280 m^2/g and between 0.103 and 0.161 cm^3/g, respectively. These values were lower than the ones corresponding to the pillared clays supports (280 and 380 m^2/g, and 0.178 and 0.216 cm^3/g). It was shown that upon impregnation and calcination the pillared clays suffered comparable microporous and mesoporous losses and

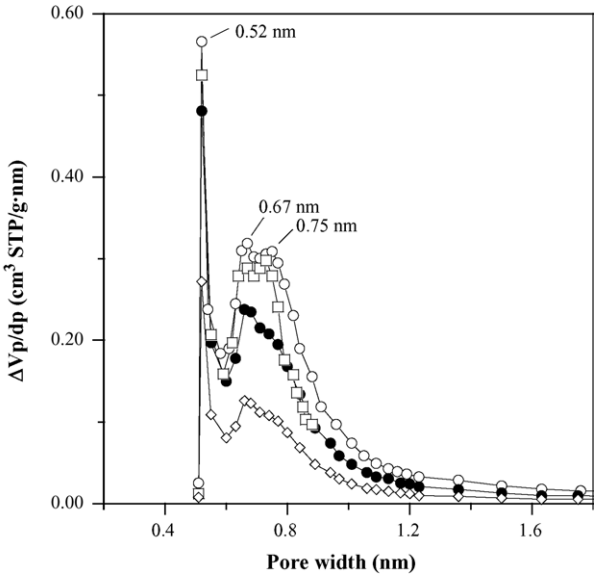

Fig. 1. Comparison of the micropore-size distributions derived from Horvath–Kawazoe (slit-like, ●), Saito–Foley (cylindrical, □) and Cheng–Yang (slit-like, ◇) pore models for Mn/GAmont-Al. The micropore-size distribution derived from Horvath–Kawazoe (○) pore model for GAmont-Al has also been included for comparison purposes.

that the whole range of micropore diameters resulted almost uniformly affected. Various methods and models have been applied to the nitrogen adsorption data for several pore geometries to characterize the microporosity of the catalysts [11,12]. In the present work, the micropore-size distributions (MPSD) derived from the models proposed by Horvath and Kawazoe (HK), Cheng and Yang (ChY) and Saito and Foley (SF) have been used to study the microporous region of the materials. A comparison of the MPSD derived from these models for Mn/GAmont-Al is shown in Fig. 1. The distributions are bimodal and do not depend on the model. It seems that the microstructure of these materials can be equally described by either slit-like or cylindrical pore geometries when nitrogen is used as the adsorbate. The distributions show a first maximum at about 0.52 nm and a second maximum at 0.67 nm. The microporous volumes ($V_{\mu p(HK)}$) calculated according the HK model and with the method proposed by Gil and Grange [13], and the maxima of the MPSD are summarised in Table 1. For comparison purposes, the microporous volumes have been also calculated by means of the Dubinin–Astakhov (DA) equation [14] in the relative pressure range between 0.01 and 0.05 ($V_{\mu p(DA)}$). Maximum pore diameters at 0.53–0.74 nm have been obtained for the samples when the Jaroniec–Gadkaree–Choma model (JGC) is considered (see Fig. 2).

The presence in the supported manganese oxide catalysts of poorly dispersed α-Mn_2O_3 (JCPDS file no. 31-0825) and β-MnO_2 (JCPDS file no. 44-0141) particles was detected by XRD [15]. The TPR patterns showed typical reduction profiles of bulk-like manganese oxide particles, two reduction peaks consistent with successive reduction of both MnO_2 and Mn_2O_3 into Mn_3O_4, followed by a final reduction to MnO [16] (see Fig. 3). The intensity of the first peak is always greater than that

Table 1
Microporous properties derived from the nitrogen adsorption at −196 °C of the samples indicated

Sample	Slit-like model			JGC model	DA equation		
	$V_{\mu p(HK)}$[a](cm^3/g)	dp_{HK}[b](nm)	dp_{ChY}[c](nm)	dp_{JGC}[d](nm)	$V_{\mu p(DA)}$[a](cm^3/g)	E[e](kJ/mol)	n[f]
BAsap-Al	0.105	0.58–1.19	0.58–0.89	0.54	0.106	18.51	2.2
Mn/BAsap-Al	0.066	0.52–1.63	0.52–0.95	0.74	0.072	16.87	1.8
BAsap-Zr	0.125	0.56–1.23	0.56–0.94	0.53	0.126	17.76	1.9
Mn/BAsap-Zr	0.110	0.57–1.63	0.57–0.95	0.64; 0.71	0.113	17.63	1.7
GAmont-Al	0.144	0.58–1.36	0.57–0.93	0.54; 0.65	0.145	20.53	1.9
Mn/GAmont-Al	0.099	0.60–1.36	0.59–0.91	0.55	0.098	19.27	2.4
GAmont-Zr	0.115	0.59–1.36	0.59–0.91	0.56	0.110	17.63	2.5
Mn/GAmont-Zr	0.080	0.58–1.63	0.58–0.90	0.58	0.079	17.76	2.1

[a] Specific micropore volumes derived from Horvath–Kawazoe (HK) model and Dubinin–Astakhov (DA) equation.
[b] Pore diameter range of the second maximum of the Horvath–Kawazoe micropore size distributions.
[c] Pore diameter range of the second maximum of the Cheng–Yang micropore size distributions.
[d] Maxima of Jaroniec–Gadkaree–Choma (JGC) micropore size distributions.
[e] Characteristic energy from Dubinin–Astakhov equation.
[f] Exponent of Dubinin–Astakhov equation.

of the second one. In both clays series, a shift in the TPR peak to lower temperatures is observed for Mn/BAsap-Zr and Mn/GAmont-Zr in comparison with the rest of catalysts. Assuming that MnO is the final product after reduction, the manganese oxide stoichiometries calculated from the integrated TPR profiles were between 1.44 and 1.93 (see Fig. 3), in accordance with the presence of Mn_2O_3 and MnO_2 mixtures. An effect of the nature of the starting smectite used and pillaring on the O/Mn ratio was found. The ratio is higher over the manganese oxide catalysts supported on Gador montmorillonite than on Ballarat saponite, and when the clays are used unpillared with respect to the pillared materials. These results indicate a higher formation/presence of MnO_2 in these catalysts during the calcination of the impregnated solids.

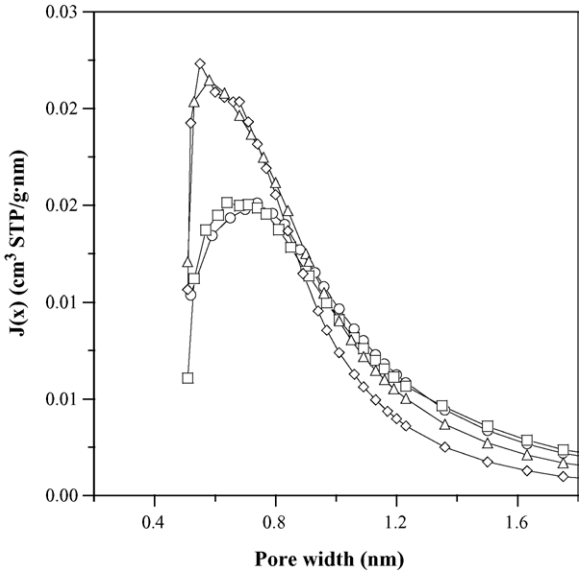

Fig. 2. Micropore-size distributions derived from the Jaroniec–Gadkaree–Choma model. (○) Mn/BAsap-Al, (□) Mn/BAsap-Zr, (◇) Mn/GAmont-Al and (△) Mn/GAmont-Zr.

The light-off curves for acetone complete oxidation revealed some interesting differences between the performances of the several Mn/PILCs catalysts [4]. According to the general behaviour of the various catalysts throughout the light-off experiments, the following order of improving catalytic

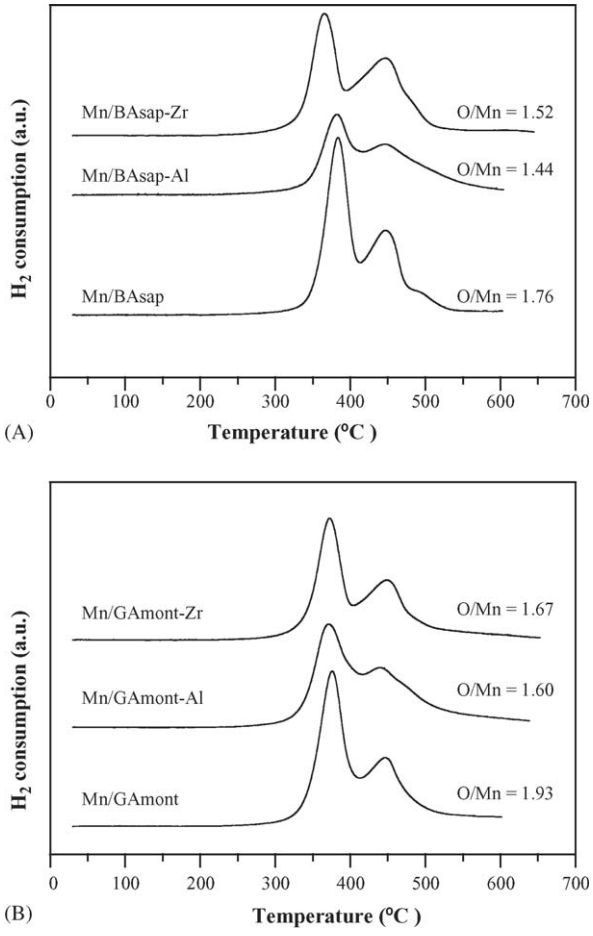

Fig. 3. TPR patterns of (A) manganese Ballarat saponites and (B) manganese Gador montmorillonites. The O/Mn ratios have also been included.

performance can be established with respect to the pillars composition: Al-pillared clays < unpillared clays < Zr-pillared clays. The temperatures required to reach complete acetone conversion are somewhat lower over the manganese oxide catalysts supported on Gador montmorillonite than on Ballarat saponite. In order to obtain more information about the effect of the support nature, a series of light-off tests was also carried out with the clay-based supports [4]. As a first result, the performance of the supports is considerably worse than that of the Mn/PILCs catalysts. The temperatures required to achieve acetone light-off over the supports are 80–160 °C higher than the ones over the supported manganese oxide catalysts. The following order of improving catalytic performance is established among the supports with respect to the pillars composition: Al-pillared clays < unpillared clays ≪ Zr-pillared clays. This sequence is the same than the above mentioned for the Mn/PILCs catalysts, which could indicate that there is an effect of the clay characteristics on the performance of these catalysts for acetone combustion.

Infrared studies on the oxidation of acetone over several oxides have shown that the combustion being produced at the expense of nucleophilic lattice oxygen species, proposing a Mars-van Krevelen type mechanism for the reaction [17]. The same group of researchers [18] have reported that carbonyl compounds carrying hydrogen atoms at their α-positions can undergo base- or acid-catalysed enolization at the surface of metal oxide base catalysts. The enolic species produced by this way are strongly bound on the catalyst surface, and can play a major role conditioning the initial interaction with the catalyst and the complete oxidation of the carbonyl reactants [18,19]. The presence of acid sites located on the pillars surface and the tetrahedral clay layers [20] influences the catalyst behaviour through the enolic species that can be performed from the acetone on the catalyst surface. These species can react as well as the gas phase molecules of the carbonyl compounds, to give aldol condensation products that can remain adsorbed on the catalyst. It may be expected that over the more acidic catalysts the aldol condensation reactions of acetone compete more efficiently with its complete oxidation, contributing to a lower combustion activity as compared to the less acidic solids. This can explain the performance exhibited in the complete oxidation of acetone by the Al-pillared clays and the Mn/Al-pillared clays catalysts, and also the better behaviour showed by the samples derived from the montmorillonite as compared to the saponite. The good performance of GAmont-Zr and BAsap-Zr could in great part be due to the activity of ZrO_2-like species present as pillars and may be also as segregated zirconia particles deposited outside the interlayer space. Accordingly, the activity of the ZrO_2-like species present could also contribute to the good performance showed by the Mn/Zr-PILC catalysts.

The Mn/pillared clays consist on supported α-Mn_2O_3 and β-MnO_2 particles as it was observed from XRD analysis and from the manganese oxide stoichiometries calculated from the integrated TPR profiles. The TPR results also indicate a higher presence of MnO_2 on Mn/GAmont and Mn/BAsap with respect to the pillared catalysts. Taking into account the ionic character of the metal–oxygen bond of these oxides, MnO_2 will be more active than Mn_2O_3 in the oxidation of acetone to CO_2. Previous catalytic run experiments performed using unsupported Mn_2O_3 and MnO_2 indicated that the main difference between the light-off curves from the single oxides was only their shape, that it is related to the reaction kinetics. No differences in the temperature of combustion were found. Therefore, the differences observed in catalyst performance cannot be mainly related to the distribution of Mn_2O_3 and MnO_2.

In conclusion, the results presented in this work indicate that the support nature and the catalyst acid-base properties can be important factors conditioning the complete oxidation of acetone on Mn/pillared clays.

Acknowledgements

Financial support by the Spanish Ministry of Education and Science and FEDER (MAT2003-01255 and MAT2002-03526) is gratefully acknowledged. S.A.K. acknowledges financial support by the Ministry of Education and Science through the Ramon-y-Cajal program.

References

[1] R. Prasad, L.A. Kennedy, E. Ruckenstein, Catal. Rev. Sci. Eng. 26 (1984) 1.
[2] M.F.M. Zwinkels, S.G. Järås, P.G. Menon, T.A. Griffin, Catal. Rev. Sci. Eng. 35 (1993) 319.
[3] J.G. McCarty, M. Gusman, D.M. Lowe, D.L. Hildenbrand, K.N. Lau, Catal. Today 47 (1999) 5.
[4] L.M. Gandía, M.A. Vicente, A. Gil, Appl. Catal. B 38 (2002) 295.
[5] P. Papaefthimiou, T. Ioannides, X.E. Verykios, Appl. Catal. B 15 (1998) 75.
[6] W. Hua, Z. Gao, Appl. Catal. B 17 (1998) 37.
[7] Y. Yazawa, H. Yoshida, N. Takagi, S. Komai, A. Satsuma, T. Hattori, J. Catal. 187 (1999) 15.
[8] A. Gil, M.A. Vicente, J.-F. Lambert, L.M. Gandía, Catal. Today 68 (2001) 41.
[9] L.M. Gandía, M.A. Vicente, A. Gil, Appl. Catal. A 196 (2000) 281.
[10] S.J. Gregg, K.S.W. Sing, Adsorption Surface Area and Porosity, Academic Press, London, 1991.
[11] A. Gil, L.M. Gandía, Chem. Eng. Sci. 58 (2003) 3059.
[12] S.A. Korili, A. Gil, Adsorption 7 (2001) 249.
[13] A. Gil, P. Grange, Langmuir 13 (1997) 4483.
[14] A. Gil, P. Grange, Colloid Surf. A 113 (1996) 39.
[15] Joint Committee on Powder Diffraction Standars, JCPDS Files, International Center for Diffraction Data, Philadelphia, USA, 1997.
[16] E.R. Stobbe, B.A. de Boer, J.W. Geus, Catal. Today 47 (1999) 161.
[17] E. Finocchio, R.J. Willey, G. Busca, V. Lorenzelli, J. Chem. Soc., Faraday Trans. 93 (1997) 175.
[18] G. Busca, E. Finocchio, G. Ramis, G. Ricchiardi, Catal. Today 32 (1996) 133.
[19] G. Busca, E. Finocchio, V. Lorenzelli, G. Ramis, M. Baldi, Catal. Today 49 (1999) 453.
[20] H.L. Del Castillo, A. Gil, P. Grange, Catal. Lett. 43 (1997) 133.